TECHNICAL MEMORANDUM

199

Assimilation of radio occultation measurements into a numerical weather prediction system

J. Eyre

Research Department

May 1994

European Centre for Medium-Range Weather Forecasts
Europäisches Zentrum für mittelfristige Wettervorhersage
Centre européen pour les prévisions météorologiques à moyen

1. INTRODUCTION

When electromagnetic radiation passes through the atmosphere it is refracted. The magnitude of the refraction depends on the gradient of refractivity normal to the path, which in turn depends on the gradients of density and the water vapour. Thus measurements of refraction will contain information on the density (and hence temperature) and the water vapour along the path. The effect is most pronounced when the radiation traverses a long atmospheric limb path, and a series of such paths at different tangent heights yields measurements containing information on the vertical profile of refractivity (see Fig 1). At radio frequencies, it is not possible to make direct and accurate measurements of the refracted angle. However, if the transmitter and receiver are in relative motion, the refraction introduces a change in the Doppler shift of the received signal, and this can be related to the refracted angle.

There were early proposals for remote sensing of the terrestrial atmosphere using such "radio occultation" or "refractometry" techniques (*Fishbach*, 1965; *Lusignan et al*, 1969). However, to date they have only been applied successfully to studies of the atmospheres of other planets (for early proposals and results, see *Fjeldbo and Eshleman*, 1965; *Kliore et al*, 1965; *Fjeldbo and Eshleman*, 1968. *Hardy et al*, 1992, give references to more recent work.) Here the transmitter is on a spacecraft orbiting the planet, and the radio signal is measured by a receiver on the Earth, having been refracted by a limb path through the planetary atmosphere. For studies of the Earth's atmosphere, equivalent measurements may be made with a transmitter on one satellite and a receiver on another.

Until recently, measurements of useful accuracy for the Earth's atmosphere were precluded by technical constraints; extremely high frequency stability is required in the signal, and the positions of the receiver and transmitter must be known to very high accuracy. With the advent of a network of Global Positioning System (GPS) satellites, together with the possibility of GPS receivers on some low Earth-orbit (LEO) satellites, it now appears that useful accuracy can be achieved (e.g. see *Hardy et al*, 1992). Each LEO can make a series of limb path measurements twice an orbit, going into and out of Earth-eclipse with respect to the GPS satellite (see Fig 2). Hardy et al calculate that, with a nominal network of 21 GPS satellites, about 600 soundings per day would be available from each LEO.

A recent and thorough study, investigating the simulation and interpretation of GPS radio occultation measurements, is reported by *Gorbunov and Sokolovskiy* (1993). Studies by *Kursinski et al* (1993a and 1993b) have also simulated many aspects of these measurements and their expected error characteristics.

Timely access to such data (assuming they are sufficiently accurate) would represent a major, new contribution to the set of observations available for operational meteorology. In particular, they could play a significant role in global numerical weather prediction (NWP). Since they would be widely distributed,

the data from even one LEO would represent a significant contribution to the global observing system. If GPS receivers were placed on many LEOs, then they would represent a very major source of information on the atmosphere's temperature and humidity fields. The aim of this paper is to explore how such observations might be used most effectively in the data assimilation process for NWP, taking into account the particular strengths and weaknesses of this type of measurement.

Most of the theoretical literature in this field has treated the processing of refractometry data as an inverse problem: given a set of measurements of refracted angle at a range of tangent heights, how do we estimate the vertical profile of refractivity (and hence density) close to the tangent point? Assuming that the set of tangent points are not significantly separated in the horizontal and that the atmosphere can be approximated locally as spherically symmetric, there is a direct and elegant solution to the inverse problem through an Abel transform (see *Fishbach*, 1965; *Fjeldbo et al*, 1971). For studies of planetary atmospheres, these approximations have been adequate, since the accuracy obtained has exceeded the accuracy of any prior information concerning these atmospheres. Moreover, in the absence of such prior information, it is not clear what better approach could have been adopted.

However, in the case of the Earth's atmosphere, we have accurate prior information on the state of the atmosphere. This is encapsulated in the short-range forecasts provided by a NWP system. These forecasts may be considered as a synthesis of all recent observations from a range of observing systems, combined together in a dynamically consistent way through the medium of the NWP model. Thus a 6-hour forecast of temperature from such a model typically has an error ~ 1 K in the troposphere and lower stratosphere. Similarly the field of specific humidity is known a priori with accuracies ranging from ~ 10% in the lower troposphere to ~ 30% in the upper troposphere. Also important, in relation to radio occultation data, is the prior knowledge of information on the horizontal gradients of these fields (i.e. on the departures from spherical symmetry). For example, in the vicinity of fronts and jet streams, horizontal gradients are not only large but reasonably well known in advance of the measurements. Because of the intrinsically low horizontal resolution of radio occultation data, there is a danger that their information could be misinterpreted, particularly in areas of strong horizontal gradient, if not assimilated into the NWP model with due regard to the true horizontal resolution and information content of the data. This is analagous to the problem encountered in the vertical when attempting to assimilate data from infra-red/microwave nadir-sounding radiometers such as TOVS. The vertical resolution of these instruments is comparable to or lower than the typical vertical scales of error in the short-range forecasts, which provide the a priori ("background") fields for NWP data assimilation. This problem has made vertical profiles of temperature/humidity retrieved from such data difficult to assimilate successfully into NWP systems, and it has led to recent moves to assimilate the radiance data themselves directly into the NWP system (e.g. see *Eyre et al*, 1993; *Andersson et al*, 1994). With radio occultation data, we may expect to experience the

equivalent problem in the horizontal, where the scales resolved by the observing system are comparable with the horizontal scales of short-range forecast error (see section 5 for examples).

A further problem concerns the inability of the radio occultation data to separate the effects of temperature and humidity, in the absence of other information. Within the context of NWP data assimilation, such information arises naturally in the form of background fields of temperature and humidity, and estimates of their expected errors.

These considerations suggest that optimal use of radio occultation data will be made if we can find a way of assimilating the measurements of refracted angle directly in the model. Recent developments in variational data assimilation have shown how this can be achieved for observations in general, if we can specify an "observation operator" which solves the "direct" problem of calculating the observation expected given the NWP model state (e.g. see *Lorenc*, 1986; *Talagrand*, 1989; *Pailleux*, 1989). In the variational approach, the inversion of each data type does not appear explicitly in the problem; the requirement is for a fast and accurate method of solving the direct problem (and its associated gradient or adjoint problem).

In section 2, the characteristics of the GPS radio occultation data are considered, and it is suggested how they might be presented for use in NWP. In section 3, the variational approach to data assimilation is presented briefly, and the options for assimilation of radio occultation data are discussed. In section 4, the theory involved in a direct model for radio occultation data is developed, first for the spherically symmetric case and then for the case where horizontal gradients are taken into account. A scheme for implementing such a direct model is presented along with ideas for further extensions to the model for use with real data. In section 5, some results from the application of the direct model are presented, demonstrating the accuracy of the scheme and the effects of neglecting horizontal gradients. The concept of a two-dimensional weighting function for radio occultation measurements is introduced, and some illustrative examples are given for temperature and humidity.

2. DATA FROM RADIO OCCULTATION MEASUREMENTS

The basic measurement is one of radio-frequency against time as the receiver goes into occultation with respect to the transmitter (see Fig 3). The relative positions and velocities of the two satellites can be computed very accurately (using data taken outside occultation). From the Doppler shift of signal f_d and a knowledge of the Earth/satellite geometry it is possible to calculate the refracted angle ε and the impact parameter p, using the following equations:

$$\varepsilon = \phi_1 + \phi_2 + \theta_1 + \theta_2 - \pi \tag{2.1}$$

$$p = r_1 \sin \phi_1 = r_2 \sin \phi_2 \tag{2.2}$$

$$f_d = f_o\, c^{-1}(v_1^r\cos\phi_1+v_2^r\cos\phi_2+v_1^c\sin\phi_1-v_2^c\sin\phi_2) \qquad (2.3)$$

where f_o is the carrier frequency, c is the speed of light, and v_i^r and v_i^c are the radial and circular components of the velocity of satellite i in the plane containing the refracted path. For further details see *Gorbunov and Sokolovskiy* (1993). Their notation and their treatment of this and other aspects of the theory have been followed where possible.

Three further problems must be addressed in practice:

a) The radio signal is refracted not only by density and water vapour gradients in the neutral atmosphere but also by gradients of electron density, which give significant effects in the ionosphere. This effect can be estimated and an adjustment made using measurements at two radio frequencies (see *Hardy et al*, 1993). For use of the refracted angle data in NWP, it would be important that this adjustment accompanied the measurement, and that an estimate of the probable error in the adjustment were made available.

b) The earth is not a sphere; the ellipsoidal shape of the Earth should be taken into account. This will include interpreting the path of the ray in terms of an effective local radius of the Earth and suitable transformations between geocentric and geodetic latitude.

c) The values of p and ε derived above are strictly valid only for local spherical symmetry (i.e. no horizontal gradients of temperature and humidity). For accurate interpretation of the data, asymmetric effects should be taken into account. These aspects are discussed further in sections 4 and 5.

To permit effective use of radio occultation data within a NWP data assimilation system, the following information should be provided: for each limb path, corresponding frequency data averaged over a suitable time interval, and the associated information on satellite geometry, should be converted to values of:

- impact parameter p,
- refracted angle ε,
- latitude and longitude of tangent point,
- direction on the Earth's surface of the plane of the measurement, and
- adjustment of ε and p for the ionosphere.

In addition, for accurate interpretation of the data, the position vectors of both satellites are required (see section 4.7).

Horizontal locations of the tangent points for different values of p may be sufficiently close that, for convenience, we can treat them all as at the same location. However, with the variational approach described below, this is not a restriction; the observations at each value of ε may be assimilated separately if necessary.

Also required for effective use of the data will be estimates of the measurement errors. These should include not only the true instrumental error but also errors arising from simplifications in the direct model. These will include uncertainties in adjustments for the effects of the ionosphere (*Kursinski et al*, 1993b) and "noise" introduced by turbulence and other unresolved features in the atmosphere's refractivity field (M Sokolovskiy, personal communication).

3. VARIATIONAL DATA ASSIMILATION

The principles of variational data assimilation have been discussed in detail elsewhere (e.g. *Lorenc*, 1986; *Le Dimet and Talagrand*, 1986). Here we present only those aspects relevant to an understanding of the options for assimilating radio occultation data.

The analysis of the atmospheric state x is found by minimizing a cost function of the form

$$J(x) = \tfrac{1}{2}(y-H\{x\})^T(O+F)^{-1}(y-H\{x\}) + \tfrac{1}{2}(x-x_b)^T B^{-1}(x-x_b) + J_c(x) \qquad (3.1)$$

where x_b is the background estimate of x (i.e. a short-range forecast),

B is the covariance of expected error in x_b,

y is a vector of observations,

$H\{x\}$ is the observation operator, which calculates the observation that would be made given the state x,

O is the covariance of expected error in the observations,

F is the covariance of expected error in the observation operator,

and $J_c(x)$ represents additional "costs", through which other dynamical or physical constraints may be imposed.

In the case of global NWP, x is a vector of variables representing the whole global atmosphere. (In the system under development at ECMWF, x includes three-dimensional fields of temperature, specific humidity and two components of wind at 31 levels in the vertical with a horizontal resolution of about 100 km. Thus it contains ~ 10^7 elements!)

$\mathbf{y}$ contains all observations made close to the time of the analysis. They are of many different types with widely varying characteristics (e.g. see *Bengtsson et al*, 1982). If the errors of different observing systems, and of different sensors within each system, are independent, then the first term in (3.1) may be split into a separate term for each group of observations (e.g. each radiosonde profile). If radio occultation data were available to add to the total set of observations, then they could be represented by additional components in the first term of cost function. Each occultation could be represented by a separate term, as its random errors would be independent of those in other occultations. [We assume here that any systematic errors are negligible or that they have been corrected through some pre-processing.]

The minimization problem represented by (3.1) is of very large dimension and is, in general, nonlinear. It must therefore be solved by numerical, iterative techniques which involve computation of the gradient of the cost function:

$$\nabla_x J(x) = -H'\{x\}^T O^{-1}(y-H\{x\}) + B^{-1}(x-x_b) + \nabla_x J_c(x). \qquad (3.2)$$

$H'\{x\}^T$ is the Jacobian matrix, $\nabla_x H\{x\}$, expressing the gradient of the observation operator with respect to each element of the state x. Because of the size of x, (3.2) cannot in general be evaluated through matrix multiplication, but through the use of adjoint equations (e.g. see *Hoffman et al*, 1992). For example, the first term is evaluated by operating on the vector $O^{-1}(y-H\{x\})$ with the adjoint of the tangent linear model associated with the direct model $H\{x\}$.

An alternative way of visualizing the variational assimilation of observations into a NWP model is shown schematically in Fig 4. Note that the comparison of measurement with model takes place in the space of the observed variables, not that of the model variables.

The options for assimilation of radio occultation data are as follows:

a) **Direct assimilation of refracted angle data**

This would have the advantage that the observations would be (apart from the ionospheric adjustment) in their "raw" form and so the error characteristics would be relatively simple. Indeed, if the errors at each point in the occultation profile were uncorrelated, they could be treated independently as scalar measurements. All we would require to specify $O+F$ would be an estimate of the random error expected in each refracted angle measurement and its associated observation operator. The complexity arises in the observation operator $H\{x\}$ which would have to perform the following operations:

- interpolate the NWP model data for temperature, humidity and pressure at each model level to values in the plane containing both satellites and the centre of the Earth,
- for a given value of the impact parameter, p, and using the meteorological variables in this plane,

calculate the expected refracted angle, ε. This aspect of the problem is considered in detail in section 4.

b) **Assimilation of retrieved profiles of refractivity**

This would be an intermediate approach. The vector of occultation measurements ε would be inverted prior to assimilation using the Abel transform to give a profile of refractivity at the tangent point. The observation operator $H\{x\}$ would interpolate the model fields to give profiles at the location of the tangent point and then derive the corresponding profile of refractivity. It would also be desirable to use a profile averaged in the horizontal over a distance comparable with the resolution of the measurements. The drawback with this approach is that unnecessary errors would be introduced through the approximations inherent in the assumption of spherical symmetry. These would also lead to vertical correlations of error in the refractivity profile, and such correlations would be difficult to specify in a general way.

c) **Assimilation of retrieved profiles of temperature and/or humidity**

This would have the advantage of the simplest observation operator, involving only interpolation of model profiles to the position of the retrieved profiles (and perhaps some horizontal smoothing as in (b)). However, in addition to the drawbacks of (b), it would also suffer from additional errors involved in resolving the ambiguity between temperature and humidity (whatever the method chosen to perform this step). Moreover the inherent ambiguity between temperature and humidity would lead to correlations of error between the retrieved temperature and humidity profile, and these correlations would also be profile-dependent. The expedient of using only temperature retrievals in the upper troposphere and stratosphere, and of using only humidity retrievals in the lower troposphere, would clearly not be an optimal use of the information.

It is clear on theoretical grounds that option (a) is preferred. However methods (b) and (c) might also be acceptable if sufficient attention were paid to the characterisation of the appropriate error covariances.

4. A DIRECT MODEL FOR REFRACTOMETRY

4.1 Theory for the general case

When electromagnetic radiation passes through a medium of varying refractivity n, its direction changes such that

$$n \sin\alpha = constant \tag{4.1}$$

where α is the angle between the path of the radiation and refractivity gradient vector. This is Snell's Law. If the path remains in one plane then the change in direction can be expressed in polar co-ordinates, using the system defined in Fig 5, as follows

$$d\varepsilon = -\frac{1}{n}\left(\frac{\partial n}{\partial r}\right)_\theta r\, d\theta + \frac{1}{n}\left(\frac{\partial n}{\partial \theta}\right)_r \frac{dr}{r}. \tag{4.2}$$

If ϕ is the angle between the path and the local radial, then

$$\tan\phi = r\frac{d\theta}{dr} \tag{4.3}$$

and $$\varepsilon = \theta + \phi - \frac{\pi}{2}. \tag{4.4}$$

Combining (4.2), (4.3) and (4.4):

$$d\theta + d\phi = \tan\phi\frac{dr}{r} + d\phi = d\varepsilon = -\frac{1}{n}\left(\frac{\partial n}{\partial r}\right)_\theta \tan\phi\, dr + \frac{1}{n}\left(\frac{\partial n}{\partial \theta}\right)_r \frac{dr}{r}. \tag{4.5}$$

4.2 Spherically symmetric case

If we can make the approximation of local spherical symmetry, $(\partial n/\partial\theta)_r = 0$, and so (4.5) gives

$$\frac{d\phi}{\tan\phi} + \frac{dr}{r} + \frac{dn}{n} = 0. \tag{4.6}$$

Integrating,

$$r\, n \sin\phi = constant = p. \tag{4.7}$$

This is known as Bouguer's formula (see *Born and Wolf*, 1980). Defining $x = rn$ and combining (4.5) and (4.7):

$$d\varepsilon = -\left(\frac{\partial \ln n}{\partial x}\right)_\theta p(x^2-p^2)^{-1/2}dx. \tag{4.8}$$

The total refracted angle is obtained by integrating over the full limb path, noting that $x=p$ at the tangent point:

$$\varepsilon(p) = \int d\varepsilon = -2p\int_p^\infty \left(\frac{\partial \ln n}{\partial x}\right)_\theta (x^2-p^2)^{-1/2}dx. \tag{4.9}$$

Previous studies have made use of the fact that this equation can be inverted directly using the Abel transform:

$$n(x) = \exp\{\pi^{-1}\int_x^\infty \varepsilon(p)(p^2-x^2)^{-1/2}dp\}, \tag{4.10}$$

i.e. under the assumption of spherical symmetry and given the profile $\varepsilon(p)$, the refractivity profile $n(x)$ can be obtained directly.

4.3 Direct problem: spherically symmetric case

Eq (4.9) cannot be integrated analytically since $n(x)$ does not in general have an analytic form; it must be evaluated numerically.

The integration can be performed by splitting the path into a number of pieces and, over each, assuming some analytic form for $(\partial \ln n/\partial x)_\theta$. Let us assume that $(n-1)$ varies exponentially with x:

$$n-1 = k_1 \exp\{-k_2(x-x_1)\} \tag{4.11}$$

where k_1 and k_2 are constants, and $n_1 = n(x_1)$, $n_2 = n(x_2)$.

Differentiating:

$$dn/dx = -k_2(n-1) \text{ or } d\ln n/dx = -k_2(n-1)/n. \tag{4.12}$$

If we approximate further:

$$\frac{d\ln n}{dx} = A + Bx, \tag{4.13}$$

then integration of (4.9) for the element of path from $x=x_1$ to $x=x_2$ gives

$$\Delta\varepsilon = -p\left[A\cosh^{-1}\left(\frac{x}{p}\right)+B(x^2-p^2)^{1/2}\right]_{x_1}^{x_2}. \tag{4.14}$$

Combining (4.13) and (4.12) for $x=x_1$ and $x=x_2$ leads to

$$A = -\alpha\left\{f_1-\frac{f_2-f_1}{x_2-x_1}x_1\right\};\ B = -\alpha\frac{f_2-f_1}{x_2-x_1} \tag{4.15}$$

where $f_i = \dfrac{n_i-1}{n_i}$ and $\alpha = -\dfrac{1}{x_2-x_1}\ln\left(\dfrac{n_2-1}{n_1-1}\right)$.

If higher accuracy were required then (4.13) could be extended with higher order terms, yielding corresponding additional terms in (4.14).

The evaluation of the direct problem in the spherically symmetric case therefore proceeds as follows:

1. Interpolate the model fields to give a profile of pressure, temperature and humidity at the location of the tangent point on some specified set of levels (e.g. the levels of the forecast model).

2. Integrate the hydrostatic equation to find the height at each level. (The geometric height, rather than the geopotential height, is required and so the apparent gravitational acceleration should vary with height and latitude.)

3. Sub-divide the layers further (if necessary — see discussion in section 5) and calculate the height z, temperature T, pressure P and specific humidity q on each level.

4. At each level calculate the refractivity

$$n = 1 + c_1 P/T + c_2 e/T^2, \tag{4.16}$$

where e is the water vapour pressure:

$$e = Pq/\{E+(1-E)q\}. \tag{4.17}$$

E is the ratio of the molecular weights of water vapour and dry air. c_1 = 7.76 x 10^{-7} K/Pa and c_2 = 3.73 x 10^{-3} K^2/Pa.

5. Given the radius of the Earth at the profile base r_o, calculate the radius at each level $r = r_o + z$ and hence the parameter $x = rn$. r_o should be the local apparent radius of curvature of the ellipsoid.

6. For each measurement $\varepsilon(p)$, find the layer containing the tangent point $x = p$.

7. For this layer and each of those above, calculate: the contribution to the refracted angle through (4.14), the value of ϕ at the top of the layer through (4.7), and the corresponding value of θ through (4.4).

8. For the layer of atmosphere above the top level, at which $x = x_1$, we can find the approximate contribution to the refracted angle by taking $(x^2-p^2)^{-1/2}$ outside the integral in (4.9):

$$\Delta\varepsilon = p(x_1^2-p^2)^{-1/2} \ln(n_1). \tag{4.18}$$

4.4 Asymmetric case

If $(\partial n/\partial\theta)_r \neq 0$, then the equivalent of (4.6) is:

$$\frac{d\phi}{\tan\phi} + \frac{dr}{r}\left(1-\frac{1}{n}\left(\frac{\partial n}{\partial\theta}\right)_r \cot\phi\right) + \frac{dn}{n} = 0. \tag{4.19}$$

Assuming that $K = \left(1-\frac{1}{n}\left(\frac{\partial n}{\partial \theta}\right)_r \cot\phi\right)$ may be approximated as constant over a layer, we obtain

$$r^K n \sin\phi = x^* \sin\phi = constant = p^* \tag{4.20}$$

where $x^* = r^K n$. This is the local and approximate equivalent of (4.7) for the asymmetric case, and may be thought of as a generalization of Bouguer's formula. The magnitudes of horizontal gradient which occur in the atmosphere lead to refracted angles which vary only slightly (~ 1%) from the symmetric case.

From equations (4.5) and (4.20) we obtain

$$d\varepsilon = -\left(\frac{\partial \ln n}{\partial x^*}\right)_\theta p^*(x^{*2}-p^{*2})^{-½}\, dx^* + \frac{1}{r}\left(\frac{\partial \ln n}{\partial \theta}\right)_r dr \tag{4.21}$$

and hence

$$\Delta\varepsilon = -p^*\left[A\cosh^{-1}\left(\frac{x^*}{p^*}\right) + B(x^{*2}-p^{*2})^{½}\right]_{x_1^*}^{x_2^*} + \frac{1}{r}\left(\frac{\partial \ln n}{\partial \theta}\right)_r (r_2-r_1) \tag{4.22}$$

where x^* replaces x in the expressions (4.15) for A, B and α, and p^* is now specific to the layer. We have also assumed that $\frac{1}{r}\left(\frac{\partial \ln n}{\partial \theta}\right)_r$ may be treated as constant for the layer.

Also,

$$\left(\frac{\partial \ln n}{\partial \theta}\right)_r = \left(\frac{\partial \ln n}{\partial \theta}\right)_l - \left(\frac{\partial \ln n}{\partial r}\right)_\theta \left(\frac{\partial r}{\partial \theta}\right)_l \tag{4.23}$$

where l denotes the levels on which the profiles at different values of θ are specified. For the layer above the top level, where $x^* = x_I^*$, we approximate

$$\Delta\varepsilon = p^*(x_I^{*2}-p^{*2})^{-½} \ln(n_I) + \frac{1}{r_I}\left(\frac{\partial \ln n_I}{\partial \theta}\right)_r \frac{1}{\alpha} \tag{4.24}$$

where $\alpha = -\frac{1}{r_I - r_{I-1}} \ln\left(\frac{n_{I-1}}{n_{I-1}-1}\right)$.

4.5 Direct problem: asymmetric case

Using the profile at the tangent point, we first perform the calculation with the symmetric approximation as 1-8 in section 4.3. Then:

9. From a set of vertical profiles in the plane of measurement, we calculate the values of n and r at each point indicated in Fig 6 by interpolating linearly in θ using the preliminary (approximate) values of θ calculated in step 7. These values will be adequate for calculating horizontal gradients to the required accuracy.

10. A finite difference form of (4.23) is then used to calculate $\left(\frac{\partial \ln n}{\partial \theta}\right)_r$ for each section of the path.

11. (4.22) is then evaluated at each layer, this time using the values of n and r along the path. An approximate value of K for the layer is calculated using the result of step 9 and the value of ϕ at the base of the layer. Values for p^* and for ϕ at the top of the layer are obtained through (4.20). This process is initialised in the layer containing the tangent point by setting $x = x^* = p^* = p$. The radius r at the tangent point is obtained by interpolating linearly in x^*. (4.24) gives the contribution above the top level.

12. This process must be performed separately for each side of the path which, in the asymmetric case, gives a different contribution to the refracted angle.

4.6 Adjustment of the parameter p

At the top level I, $p_I = n_I r_I \sin\phi_I$, which can be taken as the impact parameter at the top of the atmosphere (and at the satellite), p_s. For the asymmetric case, this is not equal to the value p at the tangent point, with which we initialised the calculation. However, it can be shown that the variation of p along the path is very small, resulting from a second order effect. Given the algorithm above, p^* varies from layer to layer as follows:

$$p^*_{j+1}/p^*_j = r_j^{(K_{j+1}-K_j)} \tag{4.25}$$

noting that K_j tends to 1 at both the tangent point and space. Although p^* is constant for a given layer, p varies across the layer; from (4.20) and (4.7) it follows that

$$p^*_j = p_j r_j^{K_j-1} = p_{j-1} r_{j-1}^{K_j-1} \tag{4.26}$$

where p and r are specified at levels. p^* and K are specified for layers, and the j th layer lies between the $(j-1)$th and j th levels. From (4.26):

$$(p_j/p_{j-1}) = (r_j/r_{j-1})^{1-K_j} = (1-(r_j-r_{j-1})/r_{j-1})^{1-K_j} \approx 1-(1-K_j)(r_j-r_{j-1})/r_{j-1} \quad (4.27)$$

Also p is not changed in crossing the boundary from one layer to the next. Therefore p varies much less along the path that does p^* (see section 5 for typical values).

4.7 Further extensions to the direct model

The direct model described above is adequate for the purposes of the simulations described in section 5. However, there are two respects in which it may not be adequate for use with real data, and for which further developments may be necessary.

Firstly, the horizontal location of the tangent point for an asymmetric atmosphere will not be the same as that calculated from the measurement geometry assuming spherical symmetry. To correct for this, an interactive method could be used in which the asymmetry of θ at the top of the atmosphere from one calculation is used to make a correction to the location of the tangent point for the next.

For the asymmetric case, the mis-location of the tangent point described above and the variation of p along the path discussed in section 4.6 are both effects that would lead to the computed ray failing to pass through the known positions of the two satellites. However, there is yet another reason why the computed ray is not appropriate in this respect, and it applies even to the symmetric case: the value of p used in the calculation is not independent of the measured value of ε but is derived together with ε using equations (2.1) to (2.3). For given satellite positions, each pair of values of ε and p are appropriate for the true state of the atmosphere but not, in general, if other states (such as the state used in the direct calculation). From equations (2.1) and (2.2), the measured value of $\varepsilon(=\varepsilon_M)$ is related to p by:

$$\varepsilon_M = \sin^{-1}\left(\frac{p}{r_1}\right) + \sin^{-1}\left(\frac{p}{r_2}\right) + \theta_1 + \theta_2 - \pi, \quad (4.28)$$

and so

$$\frac{d\varepsilon_M}{dp} = (r_1^2-p^2)^{-1/2} + (r_2^2-p^2)^{-1/2}. \quad (4.29)$$

For GPS and LEO orbital heights of 20 000 km and 800 km respectively, $d\varepsilon_M/dp$ is above 3.4×10^{-4} radians/km. For given satellite positions, measurements must lie on the line marked "M" in Fig 7. A calculated ray must also give values that lie on this line, if the ray is to pass through the two satellites. For a given atmospheric state and horizontal location of the tangent point, the calculated value of $\varepsilon(=\varepsilon_c)$ lies

on a different line: in Fig 7, "S" indicates the calculation for the spherically symmetric approximation and "A" represents the line for the (accurate) asymmetric calculation. The value of $p=p_c$, for which the calculated ray passes through the satellites, lies at the intersection of lines "M" and "A". Starting with an initial value p_o equal to the "measured" value p_M, p_c can be found, iteratively if necessary, as follows:

$$\delta p_i = \frac{\varepsilon_c(p_i) - \varepsilon_M(p_i)}{\frac{d\varepsilon_M}{dp}(p_i) - \frac{d\varepsilon_c}{dp}(p_i)} \tag{4.30}$$

and $$p_{i+1} = p_i + \delta p_i. \tag{4.31}$$

$d\varepsilon_M/dp$ is obtained from (4.29). The calculation of $d\varepsilon_c/dp$ requires the tangent-linear or adjoint model equivalent to the direct model.

The above discussion of these two problems suggests a more general way to proceed which would handle them both:

- Starting from a value of $p=p_M$ equivalent to ε_M and a horizontal location of the tangent point (s) calculated assuming spherical symmetry, apply the direct model and calculate both ε_c and the "ray departures", i.e. the distances by which the rays miss the two satellites.

- Use the tangent-linear or adjoint of the direct model to calculate the gradients of the ray departures with respect to p and s.

- Adjust the values of p and s in order to reduce the ray departures, and then repeat the calculation iteratively until the ray departures are adequately small.

This is one way in which an adequate direct model might be developed for use with real data. However other models could be used, e.g. an iterative "ray shooting" method in which the ray calculation starts at one of the satellites, rather than at the tangent point. The criteria for an acceptable direct model are that it should be fast, it should be adequately accurate (i.e. contain errors which are not greater than those in the measurements with which the calculations are compared) and it should be accompanied by associated tangent-linear and adjoint models.

5. CALCULATIONS OF REFRACTION FOR SOME SIMPLE CASES

The direct model described above has been tested on a few simple cases, to explore its accuracy and to illustrate some interesting characteristics of the data assimilation problem.

5.1 Vertical discretization

The accuracy of the direct model for a given atmospheric state is limited by the size of the vertical intervals which define the discrete layers used in the computation of refraction. The calculation can be made to any desired accuracy with adequately thin layers, but with an associated computational cost. To test the accuracy imposed by the finite layers, calculations were made for a dry, isothermal atmosphere at 250 K. In this way, no errors arise due to the vertical discretization of the atmospheric profile itself. In addition, calculations were performed for a state which was isothermal in the vertical but with a horizontal temperature gradient of 0.01 K km^{-1}. The basic profile was defined at 61 pressure levels, from 1000 hPa to 0.1 hPa, equally spaced in ln(pressure). For a dry atmosphere at 250 K, this gives a spacing between levels of 1.123 km (which is comparable to the average spacing of levels in ECMWF's operational forecast model). Each of these layers was then sub-divided into N intervals of equal thickness. Refracted angles for half-paths (i.e. tangent point to space) and for full paths were calculated for a range of parameters p from 6370 km (near surface) to 6400 km (a height of about 30 km).

Calculations for N=8 were compared with those for N=16. Fractional differences in half-path refracted angle were ~ 0.00004 (0.00012 maximum) with no horizontal gradient in temperature, and ~ 0.00015 (0.0003 maximum) with a horizontal gradient. The fractional change in refracted angle for a change in temperature of 1 K for the whole profile was found to be ~ 0.005. Therefore errors caused by the finite layering for N=8 correspond to errors in temperature of < 0.1 K.

A further test was performed using 57 levels for the same pressure range. Thus the layers differed insignificantly in thickness, but their location relative to the tangent point of each ray was changed. For N=8, this led to changes in refracted angle of the same order as those obtained by doubling the number of layers.

A value of N=8, corresponding to a height interval of about 0.14 km, was therefore considered adequate for subsequent calculations. It could however be increased if higher accuracy were deemed necessary.

5.2 Departures from spherical symmetry

A mean temperature profile for March at 40° N (from *Houghton*, 1986), interpolated to the 61 pressure levels described above, was taken as a reference vertical profile. The humidity profile was defined by a specific humidity of 6 g Kg^{-1} at 1000 hPa, falling off as (pressure)^3 until it reached a constant stratospheric value of 0.003 g Kg^{-1}. This profile is given in Table 1.

In the horizontal, the temperature was either held constant (i.e. spherical symmetry) or allowed to vary to imitate the change in temperature through a typical mid-latitude frontal system in the vicinity of a jet stream.

Fig 8 shows the cross-section used to construct the horizontal gradient. This is a section through a frontal surface as represented by a 24 h forecast from the ECMWF operational model. Values along the 500 hPa surface were read off at 100 km intervals, relative to the horizontal location chosen as the tangent point (shown in the figure). This gradient was then imposed at all levels (which is not very realistic above the tropopause, but is adequate here for illustrative purposes). The location of the tangent point was chosen to have a steep gradient on one side and almost no gradient on the other, and thus to correspond to an extreme case in terms of errors resulting from neglect of horizontal gradient.

The profile of total refracted angle for this atmospheric state is shown in Fig 9, where it is compared with the refracted angle profile for a dry isothermal atmosphere at 250 K.

The fractional errors in the full-path refracted angle resulting from neglect of the horizontal gradients are shown by the solid line in Fig 10. They are compared with changes in refracted angles resulting from two profiles of temperature perturbations:

a) an increase in temperature of 1 K at all levels (dashed line), and

b) a temperature perturbation (dotted line) defined by

$$\Delta T(P,s) = \Delta T_o \exp\left\{-\left(\frac{s-s_o}{L}\right)^2\right\}\exp\left\{-\left(\frac{\ln(P/P_o)}{H}\right)^2\right\}\left\{1-2\left(\frac{\ln(P/P_o)}{H}\right)^2\right\} \qquad (5.1)$$

where s is the horizontal distance, and s_o and P_o define the centre of the perturbation in the horizontal and vertical respectively. This perturbation was chosen to be similar in magnitude, form and scale to typical short-range forecast temperature errors. Values of L and H to define the horizontal and vertical scales were taken from *Rabier and McNally* (1993): L = 275 km and H = 0.488 for P_o = 300 hPa. s_o was taken to be at the same horizontal location as the tangent point, and ΔT_o was set to 1 K. The vertical profile of the perturbation at this location is shown at the left of Fig 10.

The refracted angle perturbation for (b) reflects principally the shape of the perturbation in the vertical gradient of temperature. The solid and dashed lines show refracted angle perturbations which are negative near the surface and become positive in the stratosphere. This reflects two conflicting effects of a change in temperature: at constant pressure an increase in temperature reduces the density but increases the pressure (and density) of the constant height surfaces above it. The latter effect increases in importance with height. The combined effect on the refracted angle is seen either for a constant temperature perturbation at all heights (dashed line) or for the introduction of a horizontal temperature gradient (solid line).

The purpose of these calculations is to demonstrate that neglecting the horizontal gradients in the calculation of refracted angle can lead to errors which are comparable with the changes in refraction expected from typical errors in short-range forecast temperature. This is true whether the temperature errors are (unrealistically) coherent in the vertical and horizontal, or whether they have a spatial pattern similar to real forecast errors. Neglecting horizontal gradients in such cases could therefore cause us to misinterpret the observation and to make an unwarranted perturbation to an otherwise accurate NWP model field.

5.3 Radio occultation weighting functions

From Eq (3.2) applied to the direct assimilation of refracted angle data we can see that the departures between measured and calculated angles are first weighted by the inverse of their expected errors, $\boldsymbol{O}^{-1}$, and then mapped back into the space of the atmospheric variables through the operator $\boldsymbol{H'\{x\}^T}$. For this illustration, we shall consider only a single measurement of refracted angle, $y = \varepsilon$, and only the atmospheric variables (temperature and humidity) in the plane of the ray. Therefore $\boldsymbol{H'\{x\}}$ reduces to a vector containing the partial derivatives, $\partial\varepsilon/\partial T_j$ and $\partial\varepsilon/dq_j$, where T_j and q_j are the temperature and specific humidity at one of the points j at which these fields are specified. In this study, these points represent a set of profiles at 61 levels in the vertical and spaced every 100 km in the horizontal (as described above). In the absence of an adjoint model to compute $\boldsymbol{H'\{x\}^T}$, we can use a "brute force" method to calculate the partial derivatives it contains; we change only one element of $\boldsymbol{T}$ or $\boldsymbol{q}$ at a time, by one unit, holding the other elements at their reference value. Thus the value of $\partial\varepsilon/\partial T_j$ and $\partial\varepsilon/dq_j$ can be calculated for all points j in the plane for a given value of p.

By analogy with passive radiometric sounding techniques, we can think of these partial derivatives as representing a two-dimensional "weighting function", defining where the information in the measurements has come from, and also how it will be mapped back through the assimilation process. Tables 2-4 show examples for the reference atmospheric state described in section 5.2 and an Earth's radius of 6370 km. The horizontal temperature departures defining the horizontal gradients are also given at the bottom of Table 2. Tables 2 and 3 give the temperature weighting functions for impact parameters of 10 km and 3 km respectively. The largest absolute values lie close to the path of the ray, with the very largest close to the tangent point, as expected. However, the pattern is complicated and can be explained as follows:

- For the layer containing the ray, there are strong contributions caused by changes in the vertical gradient of density across the layer: a positive contribution from an increase in temperature at the lower boundary, and a negative contribution from an increase at the upper boundary.

- For levels below the ray, there is a small positive contribution caused by the increase in pressure at constant height resulting from an increase in temperature below. In this illustration, the contributions in each vertical column are equal, since the levels are equally spaced in ln(pressure).

- For levels above the ray, there is no contribution vertically, but there may be some horizontally, through the interpolation of temperature to the position of the ray.

- The contributions decrease away from the tangent point, as a result of the shortening path length within each layer.

- There is a small asymmetry in the pattern resulting from the horizontal gradient.

Table 4 shows a corresponding "humidity weighting function" for an impact parameter of 3 km. The value in the table represents $\partial\varepsilon/\partial\ln(q_j) = q_j \, .\partial\varepsilon/\partial q_j$. The pattern is similar to that for temperature, but the sign is reversed in the vicinity of the ray and the relative effect of humidity below the ray is much lower.

5.4 Variation of the parameter p along the path

As indicated in section 4.6, for the asymmetric case the parameter $p = nr \sin\phi$ is not a constant along the path. However, we see from Eq (4.28) that the departure of p from the tangent point value results from a second order effect. Computation of the departures for the reference state described above showed that p varied by much less than 1 m along the whole path. The effect is therefore negligible.

6. DISCUSSION

The complexities of the patterns shown in section 5 illustrate why the assimilation of these data into a NWP model is not a straightforward matter. They also show how the variational approach to the direct assimilation of refracted angle data would map the information from each measurement of ε into the atmospheric variables in the plane of the ray. In practice this process would take place through the application of the adjoint of the direct model. Another "forward operator" would be required to interpolate NWP model variables into the plane of the ray. The adjoint of this operator would then map information from the plane back to the three-dimensional model variables. The information would be spread further, in the horizontal and vertical and to the wind field, through the second term in Eq (3.1) or Eq (3.2), which represents the constraints imposed by the background estimate of the atmospheric state and its expected error covariance, i.e. the magnitudes of the errors, their three-dimensional spatial correlation, and the correlation of errors between the different model variables.

The case investigated in section 5 does not represent a typical situation; not only are the horizontal gradients stronger than for an average cross-section through the atmosphere, but also the tangent point has been chosen to accentuate the effects of the horizontal pattern on the refracted angle. In a global data set, such cases would be a small minority. Nevertheless they are sufficiently important to be of concern. The vicinities of jet streams and fronts are active meteorological regions, where small analysis errors can often grow rapidly to dominate errors in subsequent forecasts. It is therefore important that the analysis of data in these regions is handled with particular care.

We have assumed so far that the NWP model contains a description of the atmospheric state adequate for accurate solution of the direct problem. This assumption must be qualified in three respects. Firstly, the model cannot represent phenomena smaller than its intrinsic resolution, whereas the observation is sensitive to a larger range of scales. This is a problem to some degree for all observation types and leads to so-called "errors of representativeness" which should be included as part of the combined errors in the measurement and observation operator. For radio occultation measurements, contributions will arise from turbulence and other sources of refractivity gradient not resolved by the NWP model.

Secondly, the NWP model has an upper boundary — at present, 10 hPa in the ECMWF operational model. Direct modelling for measurements with tangent points below but close to this boundary will require an estimate of the temperature above the boundary. For this aspect of the problem, a temperature profile above the upper boundary retrieved by Abelian inversion (i.e. through solution of Eq (4.10)) should be adequate.

Thirdly, the ionosphere contributes significantly to the refracted angle. Since the NWP model contains no representation of this, the problem must be addressed prior to the data being presented for assimilation. Estimates of the effects of the ionosphere on the total refracted angle and the impact parameter, as indicated in section 2, should be adequate.

7. CONCLUSIONS

Radio occultation measurements from GPS receivers offer an important new potential contribution to the global observing system. They should provide information on the atmosphere's temperature and humidity fields which is highly complementary to that available from other observing systems. However, it has been demonstrated here that the assimilation of such information into a NWP model is not straightforward and is probably best approached through direct assimilation of refracted angle data within a variational scheme. This method will allow us:

- to handle the ambiguity between temperature and humidity in an optimal way (using estimates of the prior uncertainty in each),
- to preserve correctly what the NWP model already "knows" about horizontal gradients,

- to handle the problem that the horizontal scale of the measurement is comparable with the scale of short-range forecast errors (which is the same problem that, in the vertical, has bedevilled the assimilation of passive nadir-sounding satellite data and has forced us towards direct assimilation of the radiances),
- to handle correctly the complicated relationship between the measurement and the 2D temperature/humidity field in the measurement plane,
- to handle the observation errors properly, and
- to remove the restriction that the whole occultation profile should refer to the same horizontal location.

The implementation of this approach requires a direct model that is both fast and accurate. The basis of such a model is presented here. It handles the computation of refraction for an asymmetric atmosphere in a new way, through the introduction of an approximate generalization of Bouguer's formula. Further extensions to this model for work with real data have been discussed.

The sensitivity of the direct model to the discretization of the ray path calculation has been tested, and the errors arising through neglect of horizontal gradients in the vicinities of fronts have been quantified. The information content of the radio occultation measurement has been illustrated through the concept of a two-dimensional weighting function, of which examples have been given for temperature and humidity.

The next stage in the implementation of such a scheme would involve comparison of measurements of refracted angle with corresponding values calculated from analyzed or short-range forecast fields. In this way, the error characteristics of the observations and direct model could be explored, as a prelude to data assimilation experiments.

ACKNOWLEDGMENTS

I am grateful to Dr Sergey Sokolovskiy and Dr Michael Gorbunov (Institute of Atmospheric Physics, Moscow; visiting scientists at Max-Planck-Institut für Meteorologie, Hamburg) and to Dr Dan McCleese and colleagues (JPL) for their very helpful information, comments and suggestions.

REFERENCES

Andersson, E, J Pailleux, J-N Thépaut, J R Eyre, A P McNally, G A Kelly and P Courtier, 1994: Use of cloud-cleared radiances in three/four-dimensional variational data assimilation. To appear in Q J R Meteorol Soc, April 1994.

Bengtsson, L et al, 1982: FGGE 4-dimensional data assimilation at ECMWF, Bull Am Meteorol Soc, 63, 21-43.

Born, M and E Wolf, 1980: Principles of Optics. Pergamon Press, Sixth Edition.

Eyre, J R, G A Kelly, A P McNally, E Andersson and A Persson, 1993: Assimilation of TOVS radiance information through one-dimensional variational analysis. Q J R Meteorol Soc, 119, 1427-1463.

Fishbach, F F, 1965: A satellite method for temperature and pressure below 24 km. Bull Amer Meteorol Soc, 9, 528-532.

Fjeldbo, G and V R Eshlemann, 1965: The bistatic radar-occultation method for the study of planetary atmospheres. J Geophys Res, 70, 3217-3226.

Fjeldbo, G and V R Eshlemann, 1968: The atmosphere of Mars analyzed by integral inversion of the Mariner IV occultation data. Planet Space Sci, 16, 1035-1059.

Fjeldbo, G, A J Kliore and V R Eshlemann, 1971: The neutral atmosphere of Venns as studied with the Mariner V radio occultation experiments. Astronom J, 76, 123-140.

Gorbunov, M E and S V Sokolovskiy, 1993: Remote sensing of refractivity from space for global observation of atmospheric parameters. Max-Planck-Institut für Meteorologie Report No. 119, Hamburg.

Hardy, K R, D P Hinson, G L Tyler and E R Krusinski, 1992: Atmospheric profiles from active space-based radio measurements. Prepr. 6 Conf. on Satellite Meteorology and Climatology; 5-10 January 1992; Atlanta.

Hardy, K R, G A Hajj, E R Kursinski and R Ibanez-Meier, 1993: Accuracies of atmospheric profiles obtained from GPS occultations. Prepr ION GPS-93 Conference; 22-24 Sept 1993; Salt Lake City.

Hoffman, R N, J-F Louis and T Nehrkorn, 1992: A method for implementing adjoint calculations in the discrete case. ECMWF Tech Mem 184.

Houghton, J T, 1986: The physics of atmospheres. Cambridge University Press. Second Edition.

Kliore, A, D L Cain, G S Levy, V R Eshlemann, G Fjeldbo and F D Drake, 1965: Occultation experiment: results of the first direct measurement of Mars' atmosphere and ionosphere. Science, 149, 1243-1248.

Kursinski, E R, G A Hajj and K R Hardy, 1993a: Temperature or moisture profiles from radio occultation measurements. Proc 8th Symp on Meteorological Observations and Instrumentation; Anaheim, CA; Amer Meteorol Soc, pp J153-J158.

Kursinski, E R, G A Hajj and K R Hardy, 1993b: Atmospheric profiles from radio occultation measurements of GPS satellites. SPIE Int Symp on Aerospace Science and Sensing; Orlando, Florida; 12-16 April 1993.

Le Dimet, F X and O Talagrand, 1986: Variational algorithms for analysis and assimilation of meteorological observations: theoretical aspects. Tellus, 38A, 97-110.

Lorenc, A C, 1986: Analysis methods for numerical weather prediction. Q J R Meteorol Soc, 112, 1177-1194.

Lusignan, B, G Modrell, A Morrison, J Pomalaza and S G Ungar, 1969: Sensing the Earth's atmosphere with occultation satellites. Proc IEEE, 4, 458-467.

Pailleux, J, 1989: Variational analysis: use of observations — example of clear radiances. Proc ECMWF Seminar on "Data assimilation and the use of satellite data"; 5-9 Sept 1988; Reading, UK; ECMWF Report, Vol II, pp 99-114.

Rabier, F and A P McNally, 1993: Evaluation of forecast error covariance matrix. ECMWF Tech Memo 195.

Talagrand, O, 1989: Four-dimensional variational assimilation. Proc ECMWF Seminar on "Data assimilation and the use of satellite data"; 5-9 Sept 1988; Reading, UK; ECMWF Report, Vol II, pp 1-30.

Table 1. Reference atmospheric profile

level	pressure (hPa)	temperature (K)	specific humidity (g/Kg)
1	1000.00	280.0	6.0000
2	857.69	274.0	3.7857
3	735.64	268.0	2.3886
4	630.95	261.0	1.5071
5	541.16	254.0	0.9509
6	464.15	246.0	0.6000
7	398.10	239.0	0.3785
8	341.45	231.0	0.2388
9	292.86	225.0	0.1507
10	251.18	221.0	0.0950
11	215.44	218.0	0.0600
12	184.78	216.0	0.0378
13	158.48	216.0	0.0238
14	135.93	216.0	0.0150
15	116.59	216.0	0.0095
16	100.00	215.0	0.0060
17	85.76	215.0	0.0038
18	73.56	216.0	0.0030
19	63.09	216.0	0.0030
20	54.11	216.0	0.0030
21	46.41	217.0	0.0030
22	39.81	217.0	0.0030
23	34.14	218.0	0.0030
24	29.28	219.0	0.0030
25	25.11	220.0	0.0030
26	21.54	221.0	0.0030
27	18.47	222.0	0.0030
28	15.84	223.0	0.0030
29	13.59	224.0	0.0030
30	11.65	225.0	0.0030
31	10.00	226.0	0.0030
32	8.57	229.0	0.0030
33	7.35	232.0	0.0030
34	6.31	235.0	0.0030
35	5.41	237.0	0.0030
36	4.64	240.0	0.0030
37	3.98	243.0	0.0030
38	3.41	246.0	0.0030
39	2.93	248.0	0.0030
40	2.51	251.0	0.0030
41	2.15	254.0	0.0030
42	1.85	257.0	0.0030
43	1.58	260.0	0.0030
44	1.36	262.0	0.0030
45	1.17	264.0	0.0030
46	1.00	266.0	0.0030
47	0.86	267.0	0.0030
48	0.74	267.0	0.0030
49	0.63	266.0	0.0030
50	0.54	264.0	0.0030
51	0.46	262.0	0.0030
52	0.40	260.0	0.0030
53	0.34	258.0	0.0030
54	0.29	255.0	0.0030
55	0.25	252.0	0.0030
56	0.22	249.0	0.0030
57	0.18	246.0	0.0030
58	0.16	243.0	0.0030
59	0.14	240.0	0.0030
60	0.12	237.0	0.0030
61	0.10	234.0	0.0030

Table 2. Temperature weighting function (in rad/K x 10,000,000)
for impact parameter = 6380 km,
tangent height = 9.456 km,
tangent pressure = 278 hPa

pressure (hPa)	horizontal distance from tangent point in km														
	-700	-600	-500	-400	-300	-200	-100	0	100	200	300	400	500	600	700
10	0	0	0	0	0	0	0	0	0	0	0	0	0	0	0
12	0	0	0	0	0	0	0	0	0	0	0	0	0	0	0
14	0	0	0	0	0	0	0	0	0	0	0	0	0	0	0
16	0	0	0	0	0	0	0	0	0	0	0	0	0	0	0
18	0	0	-1	0	0	0	0	0	0	0	0	0	-1	0	0
22	0	0	-1	1	0	0	0	0	0	0	0	0	-1	0	0
25	0	0	-1	1	0	0	0	0	0	0	0	1	-1	0	0
29	0	0	-1	1	0	0	0	0	0	0	0	1	-1	0	0
34	0	0	-1	1	0	0	0	0	0	0	0	1	-1	0	0
40	0	0	-1	1	0	0	0	0	0	0	0	1	-1	0	0
46	0	0	0	-2	2	0	0	0	0	0	2	-1	0	0	0
54	0	0	1	-3	3	0	0	0	0	0	2	-3	1	0	0
63	0	0	1	-4	3	0	0	0	0	0	3	-3	1	0	0
74	0	0	1	-4	4	0	0	0	0	0	4	-4	1	0	0
86	0	0	1	-5	5	0	0	0	0	0	5	-5	1	0	0
100	0	0	1	-2	-2	5	0	0	0	4	-2	-2	1	0	0
117	0	0	1	2	-12	12	0	0	0	11	-11	2	1	0	0
136	0	0	1	2	-16	17	0	0	0	16	-15	2	1	0	0
158	0	0	1	2	-21	25	1	0	1	24	-20	2	1	0	0
185	0	0	1	2	-5	-17	35	0	35	-16	-4	2	1	0	0
215	0	0	1	2	4	-66	103	0	104	-64	4	2	1	0	0
251	0	0	1	2	4	-52	-50	539	-52	-51	4	2	1	0	0
293	0	0	1	2	4	6	-187	-689	-183	6	4	2	1	0	0
341	0	0	1	2	4	6	6	11	6	6	4	2	1	0	0
398	0	0	1	2	4	6	6	11	6	6	4	2	1	0	0
464	0	0	1	2	4	6	6	11	6	6	4	2	1	0	0
541	0	0	1	2	4	6	6	11	6	6	4	2	1	0	0
631	0	0	1	2	4	6	6	11	6	6	4	2	1	0	0
736	0	0	1	2	4	6	6	11	6	6	4	2	1	0	0
858	0	0	1	2	4	6	6	11	6	6	4	2	1	0	0
1000	0	0	0	1	2	3	3	5	3	3	2	1	0	0	0

horizontal temperature departures (K)														
1.	0.5	0.	0.	0.	0.	0.	0.	2.	5.	8.	11.	12.	13.	13.5

Table 3. Temperature weighting function (in rad/K x 10,000,000)
for impact parameter = 6373 km,
tangent height = 1.304 km,
tangent pressure = 850 hPa

pressure (hPa)	horizontal distance from tangent point in km														
	-700	-600	-500	-400	-300	-200	-100	0	100	200	300	400	500	600	700
10	0	0	0	0	0	0	0	0	0	0	0	0	0	0	0
12	0	0	0	0	0	0	0	0	0	0	0	0	0	0	0
14	0	0	0	0	0	0	0	0	0	0	0	0	0	0	0
16	0	0	0	0	0	0	0	0	0	0	0	0	0	0	0
18	0	0	0	0	0	0	0	0	0	0	0	0	0	0	0
22	0	0	0	0	0	0	0	0	0	0	0	0	0	0	0
25	0	-1	0	0	0	0	0	0	0	0	0	0	0	-1	0
29	0	-1	1	0	0	0	0	0	0	0	0	0	1	-1	0
34	0	-1	1	0	0	0	0	0	0	0	0	0	1	-1	0
40	0	-1	1	0	0	0	0	0	0	0	0	0	1	-1	0
46	0	-1	1	0	0	0	0	0	0	0	0	0	1	-1	0
54	0	-1	1	0	0	0	0	0	0	0	0	0	1	-1	0
63	0	-1	1	0	0	0	0	0	0	0	0	0	1	-1	0
74	0	-1	0	1	0	0	0	0	0	0	0	1	0	-1	0
86	0	1	-4	3	0	0	0	0	0	0	0	3	-3	1	0
100	0	1	-5	3	0	0	0	0	0	0	0	3	-4	1	0
117	0	1	-5	4	0	0	0	0	0	0	0	4	-4	1	0
136	0	1	-6	5	0	0	0	0	0	0	0	4	-5	1	0
158	0	1	-7	6	0	0	0	0	0	0	0	5	-6	1	0
185	0	1	-6	5	1	0	0	0	0	0	1	5	-6	1	0
215	0	1	2	-13	12	0	0	0	0	0	11	-12	2	1	0
251	0	1	4	-19	16	0	0	0	0	0	15	-17	3	1	0
293	0	1	4	-23	21	0	0	0	0	0	20	-20	3	1	0
341	0	1	4	-28	29	0	0	0	0	0	27	-26	3	1	0
398	0	1	4	-15	-4	24	0	0	0	23	-3	-14	3	1	0
464	0	1	4	5	-60	66	0	0	0	63	-55	5	3	1	0
541	0	1	4	5	-91	113	2	-1	2	108	-85	5	3	1	0
631	0	1	4	5	-40	-45	162	-1	159	-43	-37	5	3	1	0
736	0	1	4	5	10	-303	350	1342	343	-290	9	5	3	1	0
858	0	1	4	5	10	-31	-798	-1805	-785	-29	9	5	3	1	0
1000	0	1	2	3	5	12	15	15	17	12	5	3	2	0	0

Table 4. Weighting function of ln(specific humidity) (in rad x 1,000,000)
for impact parameter = 6373 km
tangent height = 1.304 km
tangent pressure = 850 hPa

	horizontal distance from tangent point (km)														
	-700	-600	-500	-400	-300	-200	-100	0	100	200	300	400	500	600	700
pressure (hPa)															
10	0	0	0	0	0	0	0	0	0	0	0	0	0	0	0
12	0	0	0	0	0	0	0	0	0	0	0	0	0	0	0
14	0	0	0	0	0	0	0	0	0	0	0	0	0	0	0
16	0	0	0	0	0	0	0	0	0	0	0	0	0	0	0
18	0	0	0	0	0	0	0	0	0	0	0	0	0	0	0
22	0	0	0	0	0	0	0	0	0	0	0	0	0	0	0
25	0	0	0	0	0	0	0	0	0	0	0	0	0	0	0
29	0	0	0	0	0	0	0	0	0	0	0	0	0	0	0
34	0	0	0	0	0	0	0	0	0	0	0	0	0	0	0
40	0	0	0	0	0	0	0	0	0	0	0	0	0	0	0
46	0	0	0	0	0	0	0	0	0	0	0	0	0	0	0
54	0	0	0	0	0	0	0	0	0	0	0	0	0	0	0
63	0	0	0	0	0	0	0	0	0	0	0	0	0	0	0
74	0	0	0	0	0	0	0	0	0	0	0	0	0	0	0
86	0	0	0	0	0	0	0	0	0	0	0	0	0	0	0
100	0	0	0	0	0	0	0	0	0	0	0	0	0	0	0
117	0	0	0	0	0	0	0	0	0	0	0	0	0	0	0
136	0	0	0	0	0	0	0	0	0	0	0	0	0	0	0
158	0	0	0	0	0	0	0	0	0	0	0	0	0	0	0
185	0	0	0	0	0	0	0	0	0	0	0	0	0	0	0
215	0	0	0	0	-1	0	0	0	0	0	-1	0	0	0	0
251	0	0	0	1	-2	0	0	0	0	0	-1	1	0	0	0
293	0	0	0	2	-3	0	0	0	0	0	-3	2	0	0	0
341	0	0	0	6	-8	0	0	0	0	0	-7	5	0	0	0
398	0	0	0	6	-4	-7	0	0	0	-7	-3	6	0	0	0
464	0	0	0	0	22	-35	0	0	0	-33	21	0	0	0	0
541	0	0	0	0	64	-98	-1	0	-1	-94	60	0	0	0	0
631	0	0	0	0	55	9	-189	0	-186	8	51	0	0	0	0
736	0	0	0	0	0	505	-718	-2232	-703	485	0	0	0	0	0
858	0	0	0	0	1	147	1971	4047	1948	141	1	0	0	0	0
1000	0	0	0	0	1	1	2	2	2	1	1	0	0	0	0

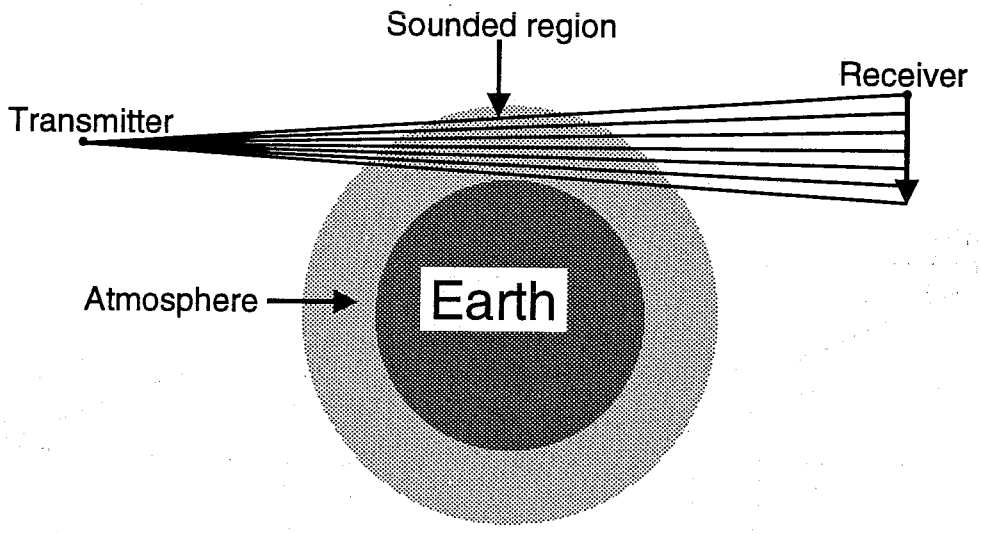

Fig 1 Illustrating the concept of refractivity profiling using radio occultation measurements. (From *Gorbunov and Sokolovskiy*, 1993).

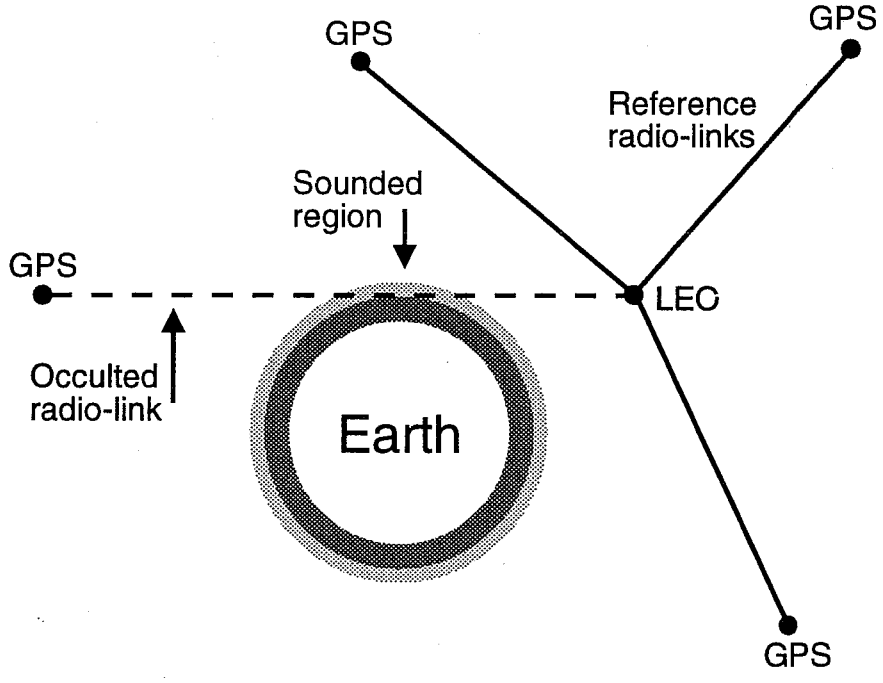

Fig 2 Illustrating radio occultation by one GEO satellite using a number of GPS satellites. (From *Gorbunov and Sokolovskiy*, 1993).

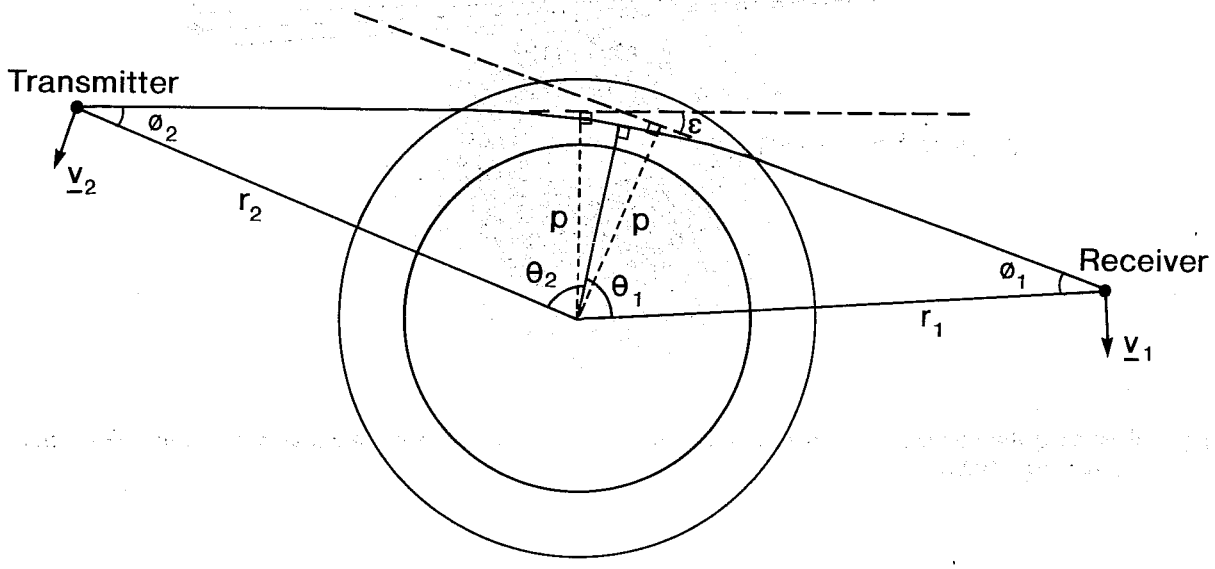

Fig 3 Defining the geometry of radio occultation measurements.

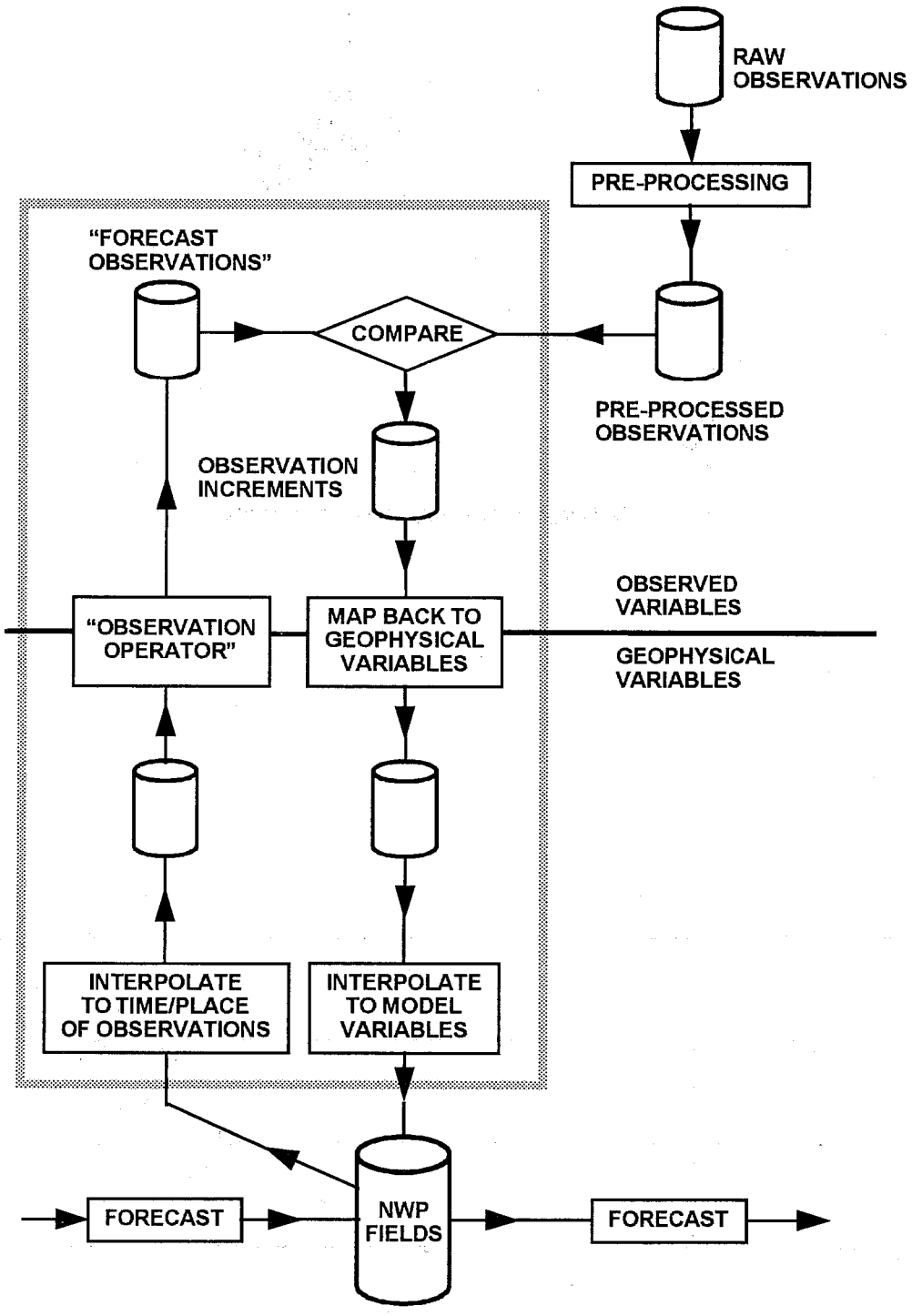

Fig 4 Illustrating the variational assimilation of observations into a NWP model.

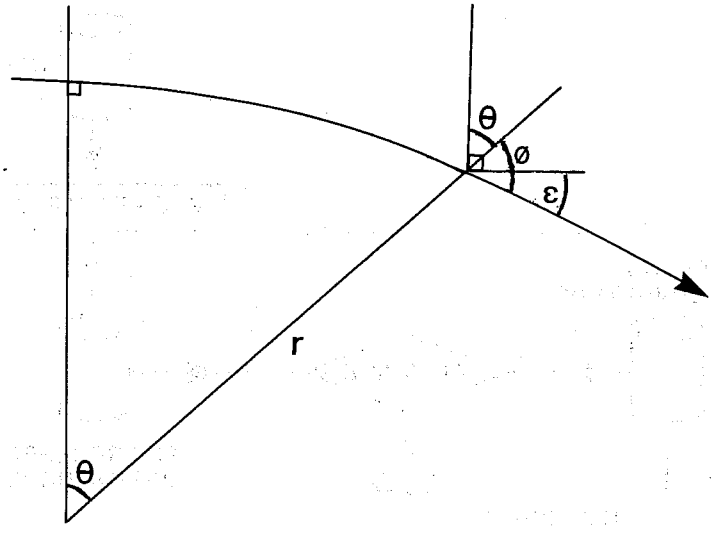

Fig 5 Defining the geometry of the direct model.

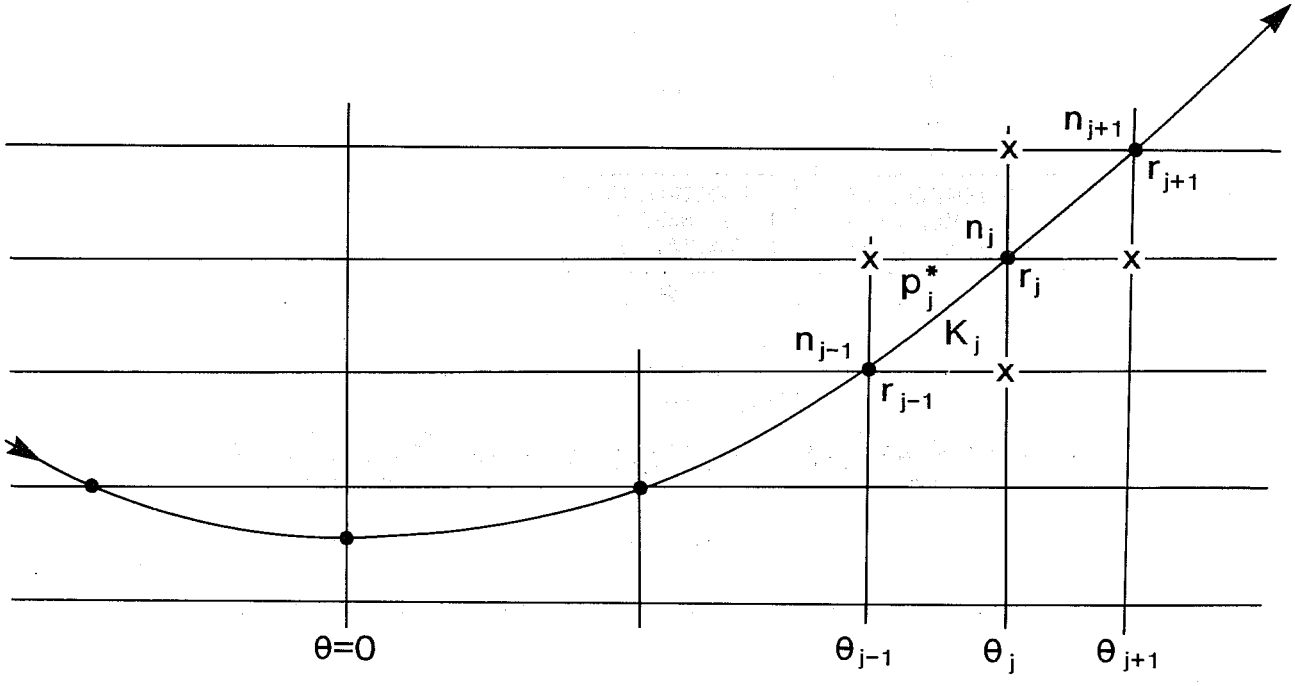

Fig 6 Illustrating the grid used in the calculation of atmospheric parameters for the asymmetric case. Points marked "•" define the path of the ray. Values at points marked "x" are also required for computation of the horizontal gradients.

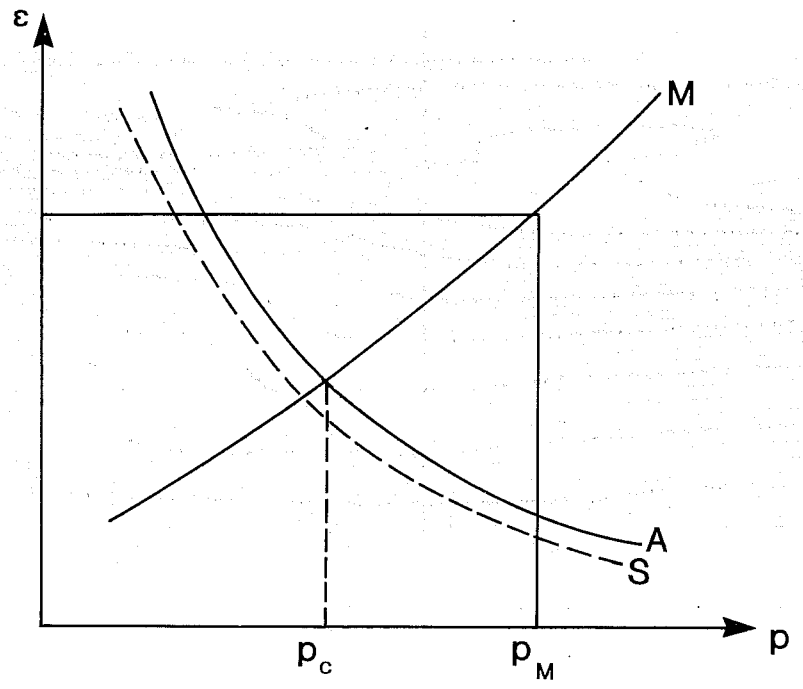

Fig 7 Illustrating the relationships between refracted angle, ε, and impact parameter, p, for measurement (line "M") and calculation ("S" for symmetric approximation, "A" for asymmetric calculation).

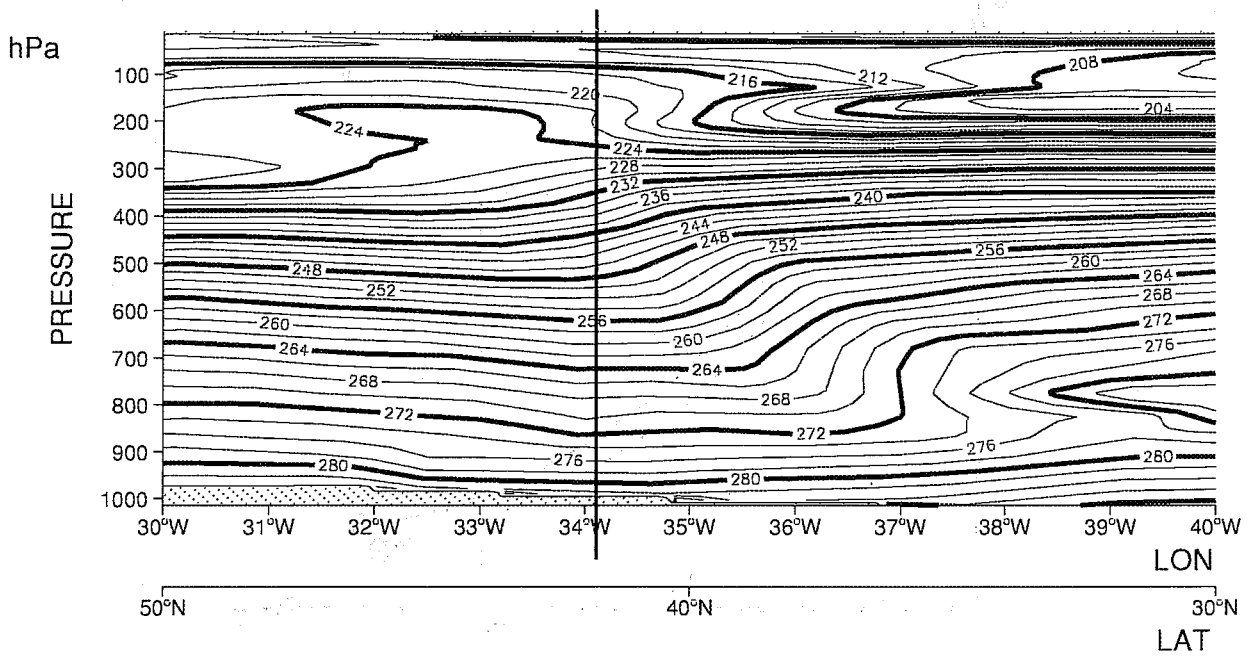

Fig 8 Cross-section of temperature (in K) through a mid-latitude frontal system as represented by a 24-hour forecast from the ECMWF operational model. 50°N, 30°W to 30°N, 40°W at 1200 on 24 February 1994. The vertical line at 34.1°W represents the position chosen for the tangent point.

Fig 9 Refracted angle versus impact parameter for the reference atmospheric state described in the text (thick line) and a dry isothermal atmosphere at 250 K (thin line).

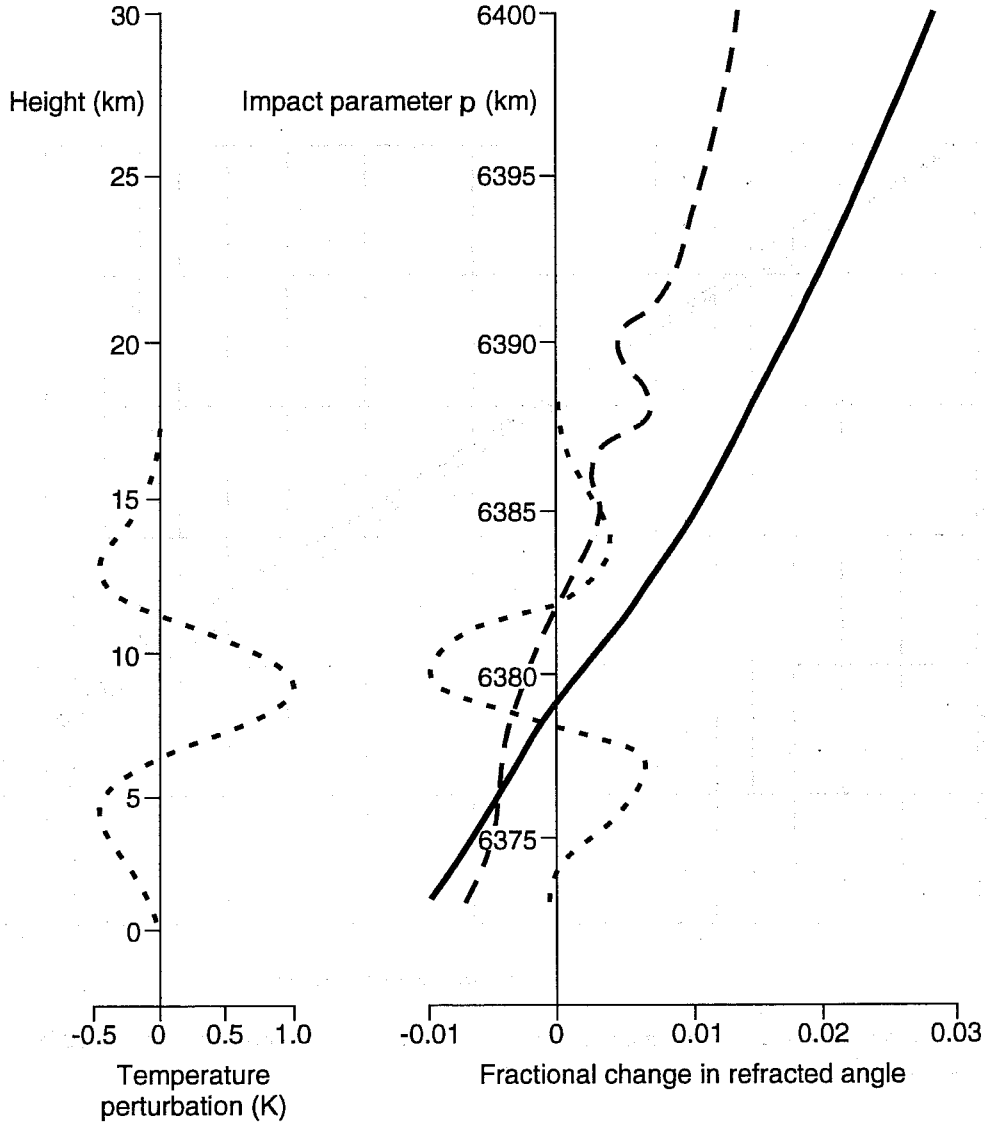

Fig 10 Comparing fractional changes in refracted angle. Solid line: the effect of neglecting horizontal gradients; dashed line: the effect of a 1 K change of temperature at all levels; dotted line: the effect of a "forecast error" temperature perturbation as described in the text. The perturbation profile at the tangent point location is shown on the left. The height scale corresponds to the impact parameter scale for the reference profile. Earth's radius taken as 6370 km.